QUARTERLY JOURNAL OF THE ROYAL METEOROLOGICAL SOCIETY
Q. J. R. Meteorol. Soc. **135**: 1336–1349 (2009)
Published online 18 June 2009 in Wiley InterScience
(www.interscience.wiley.com) DOI: 10.1002/qj.433

An analytical model for the rapid intensification of tropical cyclones

Chanh Q. Kieu* and Da-Lin Zhang
Department of Atmospheric and Oceanic Science, University of Maryland, College Park, Maryland, USA

ABSTRACT: The nonlinearity and complexity of the primitive equations have been key obstacles to our understanding of tropical cyclones (TCs), particularly in relation to the dynamical processes leading to their rapid intensification. In this study, an axisymmetric model, in which all nonlinear terms in the horizontal momentum equations are retained, is used to examine analytically the effects of organized deep convection on TC rapid intensification. By prescribing a vertical profile of the vertical motion with exponential growth in the core region, a class of exact time-dependent solutions for the primary circulations of TCs are obtained. The analytical solutions are shown to capture well many observed dynamical structures in both the core and outer regions and the rapid growth of TCs in terms of maximum winds and central pressure drops.

The analytical solutions reveal that (1) the rotational flows in the inner-core region grow double-exponentially, and the central pressure drops occur at rates much faster than the rotational growth; (2) the amplification rates of the primary circulations differ profoundly from those of the secondary circulations; (3) the rotational flows tend to grow from the bottom upwards with the fastest growth occurring at the lowest levels; and (4) the TC growth rates depend critically on the vertical structure of tangential flows, with a faster rate for a lower-level peak rotation. The nonlinear dynamics are shown to play an important role in the rapid growth of TCs. It is demonstrated that the analytical solutions can also be used to construct dynamically consistent vortices for the initialization of TC models. Limitations and possible improvements of the analytical model are also discussed.

KEY WORDS tropical cyclone growth; vortex bogussing; vortex dynamics

Received 15 September 2008; Revised 9 April 2009; Accepted 20 April 2009

1. Introduction

Despite considerable research in the past decades, our understanding of tropical cyclone (TC) development still remains elusive, especially on the dynamical processes leading to the rapid intensification of TCs. Most of our current knowledge about the TC development is based on limited observations and high-resolution modelling studies. Previous studies show that rapid deepening of TCs often occurs in relation to intense latent heat release in a weak-sheared environment with an underlying warm ocean surface (e.g. Gray, 1979). However, little is understood about why some TCs could deepen so rapidly, e.g. with the surface central pressure deepening rates ranging from 1.5 hPa h^{-1} for hurricane *Andrew* of 1992 (Liu *et al.*, 1997) to 9 hPa h^{-1} for *Wilma* of 2005 (Figure 1); the period of such rapid deepening may last from a few hours to 2–3 days. In particular, it is unclear why the rotational flows in the inner-core region grow much faster than those in the outer region (Willoughby, 1990a). This lack of understanding can be attributed to the insurmountable complexity of the primitive equations that prevents us from obtaining an analytical description of both dynamics and thermodynamics taking place during the rapid deepening stage of TCs.

Perhaps the earliest analytical approach to the problem of TC development was formulated in the framework of conditional instability of the second kind (CISK) attributing the cooperative TC growth between the frictional convergence and latent heat release (Charney and Eliassen, 1964; Ooyama, 1969). In this theory, the secondary circulation (SC), consisting of the convergent inflow in the planetary boundary layer (PBL), vertical motion in the inner-core region and divergent outflow aloft, is treated as a linear perturbation superimposed on a balanced vortex or primary circulation (PC). With an assumption that the CISK feedback occurs only within a central cloud region of a fixed radius, an explicit solution for the SC is found, which shows an exponential growth of the SC with the growth rate depending on the scale of the cloud region. Under the quasi-balanced dynamics, studies of TC development are, nonetheless, often based on the Sawyer–Eliassen equation, which was first introduced by Eliassen (1952) and later extended by Sundqvist (1970), Willoughby (1979), Shapiro and Willoughby (1982), Schubert and Hack (1982), and Hack and Schubert (1986). By prescribing a top-hat heating profile, Schubert and Hack (1982) obtained an analytical solution of the Sawyer–Eliassen equation for an invisid barotropic axisymmetric vortex, which reveals a larger temperature tendency inside the radius of maximum wind

*Correspondence to: Dr. Chanh Q. Kieu, Department of Atmospheric and Oceanic Science, University of Maryland, College Park, Maryland 20742-2425, USA. E-mail: kieucq@atmos.umd.edu

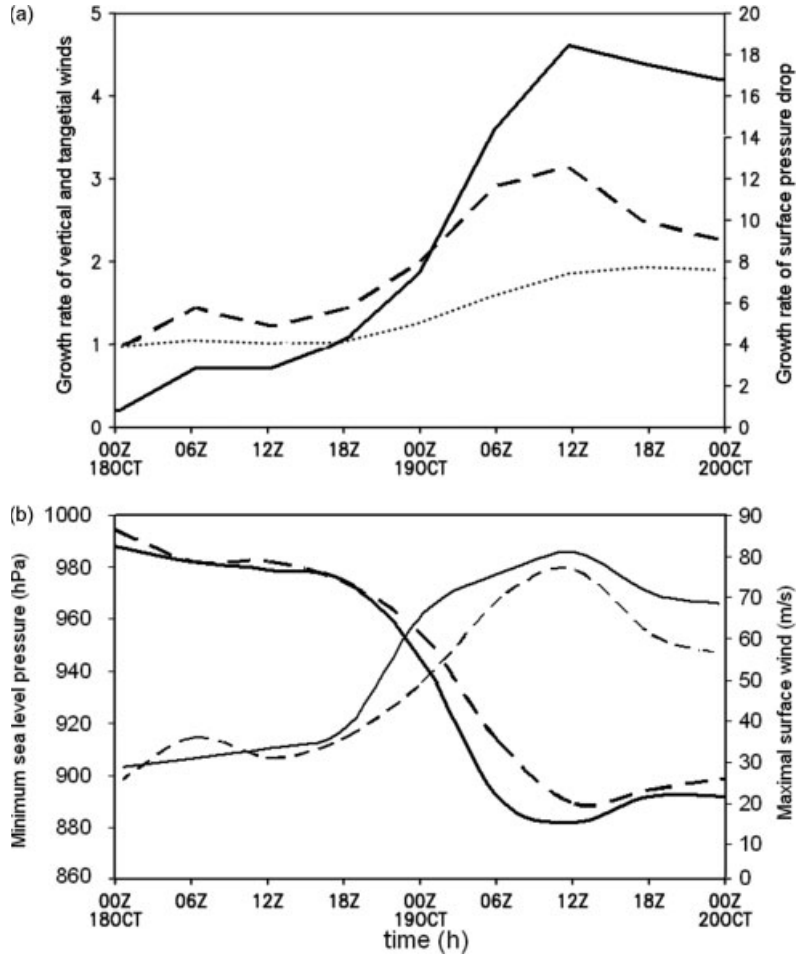

Figure 1. Time series (at 6-hour intervals) of (a) the growth rates of the r = 400 km area-averaged peak vertical motion (dotted), maximum tangential wind (dashed), and surface central-pressure drop (solid); and (b) the simulated minimum surface pressure (hPa, bold dashed) and maximum surface wind (m s^{-1}, thin dashed) versus the best track analysis (solid) from the 54-hour simulation of hurricane *Wilma* (2005), initialized at1800 UTC on 17 October 2005. The growth rates in (a) are defined with respect to their magnitudes at $t = 6$ hours into the simulation.

(RMW) than that outside. They inferred that this would cause a faster growth rate of tangential winds inside the RMW due to the presence of stronger inertial stability, and lead to the collapse of the RMW and the subsequent formation of an eye. This speculation was later demonstrated by Hack and Schubert's (1986) quasi-balanced numerical model for a nonlinear baroclinic vortex using a time-invariant Gaussian heating function, but the analytical understanding of TC growth remains unresolved.

A more acceptable theory of TC growth should take into account the air–sea interaction, the so-called wind-induced surface heat exchange processes (WISHE) after Emanuel (1989), which was initially addressed by Yanai (1964), and later extended by Emanuel (1986) with steady-state solutions for mature TCs, and Rotunno and Emanuel (1987) with an axisymmetric numerical model. An important result of the WISHE theory is the dependence of the maximum potential intensity (MPI) on the drag exchange coefficients of heat and momentum, and on the temperature difference between the PBL top and the upper-level outflows, assuming neutral slantwise ascent in the hurricane eyewall. While the WISHE theory is widely accepted as the dominant mechanism for TC genesis, explicitly time-dependent solutions have not been developed except for analytical formulations during the mature stage; Craig and Gray (1996) provide a comparative analysis of CISK and WISHE associated with TC intensification.

To date, theoretical studies of TC development appear to rely critically on the steady evolution of weak SCs under the quasi-balanced dynamics to characterize TC growth. However, none of the existing theories could be used to describe the rapid intensification of TCs in terms of central pressure drops and rotational growth, and relate them to the development of SCs. To see this, Figure 1(a) shows the growth rates of the area-averaged peak vertical motion W_{MAX}, the maximum tangential wind V_{MAX}, and the surface central pressure drop δp_{min} from a cloud-resolving simulation of hurricane *Wilma* (2005) with the Weather Research and Forecast (WRF) model at the finest resolution of 2 km. (A more detailed description of the case simulation will appear in a forthcoming paper by H. Chen and D.-L. Zhang.) The WRF model reproduces reasonably well the track and rapid intensification of the storm, including the maximum surface wind of about 80 m s^{-1}; the simulated minimum central pressure is only

DOI: 10.1002/qj

about 4 hPa weaker than the observed with a 4–5 hour lag (Figure 1(b)). While W_{MAX} begins to increase slowly after 1200 UTC on 18 October with a total increase of 60% during the rapid deepening period of 1800 UTC 18 October to 1200 UTC 19 October (Figure 1(b)), both the rotational flow and the surface central pressure drop show much faster growths, with their magnitudes amplified by about 2.5 and 4.5 times during the 18-hour deepening period, respectively. Such remarkably different growth rates of the PC and SC signify some fundamental dynamics taking place during the rapid deepening stage that has not been addressed previously.

The purpose of the present study is to investigate the rapid intensification of TCs from the perspectives of rotational growth and central pressure falls. This will be achieved by deriving a class of exact solutions to a simplified version of the primitive equations.

The next section describes the theoretical framework and the assumptions used to simplify the primitive equations. Section 3 shows derivation of the analytical solutions, given a top-hat forcing function for the vertical motion. Section 4 presents verification of the analytical solutions against some well-documented TC structures and evolution. Section 5 shows how our analytical solutions can be used to assist in the initialization of TC models. Concluding remarks are given in the final section.

2. Theoretical framework

We start from the non-hydrostatic, anelastic primitive equations in the log-pressure (p) cylindrical coordinates (r, φ, z), following Willoughby (1979),

$$\frac{\partial u}{\partial t}+u\frac{\partial u}{\partial r}+\frac{v}{r}\frac{\partial u}{\partial \varphi}+w\frac{\partial u}{\partial z}-\frac{v^2}{r}=-\frac{\partial \phi}{\partial r}+fv+F_u, \tag{1}$$

$$\frac{\partial v}{\partial t}+u\frac{\partial v}{\partial r}+\frac{v}{r}\frac{\partial v}{\partial \varphi}+w\frac{\partial v}{\partial z}+\frac{uv}{r}=-\frac{1}{r}\frac{\partial \phi}{\partial \varphi}-fu+F_v, \tag{2}$$

$$\frac{\partial w}{\partial t}+u\frac{\partial w}{\partial r}+\frac{v}{r}\frac{\partial w}{\partial \varphi}+w\frac{\partial w}{\partial z}=-\frac{\partial \phi}{\partial z}+b+F_w, \tag{3}$$

$$\frac{1}{r}\frac{\partial}{\partial r}(ru)+\frac{1}{r}\frac{\partial v}{\partial \varphi}+\frac{\partial w}{\partial z}-Sw=0, \tag{4}$$

$$\frac{\partial b}{\partial t}+u\frac{\partial b}{\partial r}+\frac{v}{r}\frac{\partial b}{\partial \varphi}+N^2w=\frac{Jg}{\overline{T}}, \tag{5}$$

where $z=-H\ \ln\ (p/p_s)$, H is the scale height, p_s is a reference pressure; u, v, and w are, respectively, the velocity component in the radial, tangential and vertical directions; ϕ is the geopotential height perturbation from its reference value $\overline{\phi}(z)$; $b\equiv gT'/\overline{T}(z)$ is the buoyancy; f is the Coriolis parameter; N is the buoyancy frequency; $S=-(1/\rho)\partial\rho/\partial z\equiv N^2/g$ is a stratification parameter; J denotes the diabatic heating rate; $F_{u,v,w}$ denote the frictional effects in the PBL. For the convenience of our derivation, parameters f and N will be treated as constants.

Due to their high nonlinearity, it is virtually impossible to obtain directly analytical solutions for Equations (1)–(5), even when the diabatic heating rate and frictional forcing are parametrized. However, as a first step, we may simplify the above equations system by assuming that a time-dependent solution for the vertical motion in a TC can be given *a priori*. Zhang *et al.* (2002) have shown that the vertical profiles of the vertical motions are similar to those of the diabatic heating rates from the thermodynamic budget analysis of a cloud-resolving simulation of hurricane *Andrew* (1992) (Figures 1(a) and 2(b) therein). This suggests that if the time evolution of the vertical motion field is known, complicated moist thermodynamical processes could be plausibly bypassed and the TC intensification could be explored in the context of pure rotational dynamics. In this regard, numerical (dry) modelling studies of Pandya and Durran (1996), and Pandya *et al.* (2000) have revealed many fundamental squall-line structures as forced by a specified vertical profile of convective heating along the leading convective line.

Under the quasi-balanced constraint, Charney and Elliasen (1964), Yanai (1964), and Ooyama (1969) established a theoretical framework for which the SC growth could be described in terms of an instability mode. That is, the diabatically induced ascending motion can be expressed as:

$$w(\mathrm{r,z,t})=\begin{cases} W_0\sin(\lambda z)\mathrm{e}^{\beta t} & r\le a\ \text{(region I)}\\ 0 & r>a\ \text{(region II)}, \end{cases} \tag{6}$$

where a is a radius characterizing the horizontal scale of TCs, W_0 and $\lambda=\pi/H_0$ are constants, and β is the growth rate of the vertical motion. The parameter β depends on various factors, such as frictional convergence and surface heat fluxes, and it is typically on the order of $10^{-6}-10^{-5}$ s^{-1} (Ooyama, 1969). Strictly speaking, β should be a function of z, and similarly for N, but it can always be approximated as a constant, at least to the leading order of the WKB expansion. This approximation amounts to a constant deepening rate of TCs in the vertical, which is not a severe constraint as TCs often show a near-constant growth rate at all levels. To see this point, Figure 2 shows the simulated time series of the deepening of hurricane *Wilma* (2005) at three different vertical (i.e. lower, middle and upper) levels. The central pressure time series (and deepening rates) are similar at all the levels, only with slight differences after the 24-hour integration.

Note that the exponential form of w as given by (6) is not a serious limitation as, to the first-order expansion, such exponential growth can always be truncated as a linear function. For example, the time series of w in Figure 1(b) shows a linear growth with $\beta\approx 2\times 10^{-6}$ s^{-1} during the intensifying period. To ease the subsequent derivations, the exponential form as given in (6) is chosen for the present study. Our purpose here is to examine how the PCs will evolve with time if the SCs grow exponentially as often assumed in previous studies. Of course, such exponential growth will no longer be valid as

DOI: 10.1002/qj

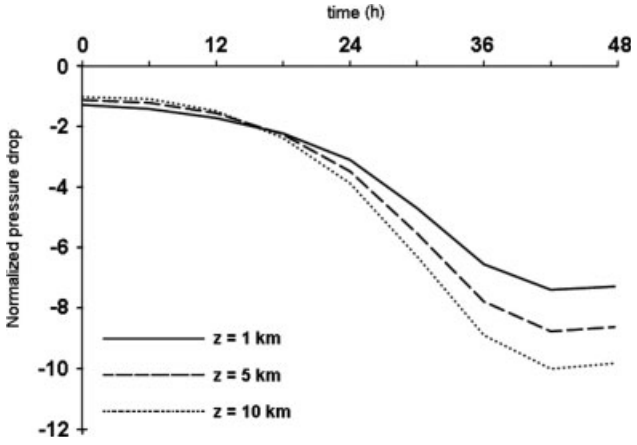

Figure 2. Time series of the pressure deviation at three different levels: $z = 1$ km (solid), 5 km (dashed) and 10 km (dotted) from the simulation of hurricane *Wilma* (2005) using the WRF model. All pressure deviations are normalized to their values at $t = 0$.

TCs reach their maximum intensity, so solution (6) should be limited to the rapid intensifying period only.

As a second step to find the analytical solutions, we make the following two assumptions: (i) TCs are axisymmetric; and (ii) only the first-order frictional effects are considered, i.e. $F_{u,v} = \kappa(u, v)$. Assumption (i) is invoked because TCs often show their consistent axisymmetric structure during the rapid intensification period and later mature stage. Apparently, considerable asymmetries related to numerous factors such as vertical wind shear, intrinsic vortex-wave interactions associated with the highly rotational flows, or inhomogeneities in the atmosphere are always observed, and they can be in principle incorporated into our model in some form of '*parametrization*'. However, this will result in a very challenging set of equations such that there is little hope for obtaining the exact solutions. Because of this, we hereafter restrict our model only to axisymmetric vortices. Assumption (ii) is adopted in order to simplify our derivation of the analytical solutions. With the above assumptions, the system of equations that we will work with is reduced to:

$$\frac{\partial u}{\partial t} + u\frac{\partial u}{\partial r} + w\frac{\partial u}{\partial z} - \frac{v^2}{r} = -\frac{\partial \phi}{\partial r} + fv - \kappa u, \qquad (1')$$

$$\frac{\partial v}{\partial t} + u\frac{\partial v}{\partial r} + w\frac{\partial v}{\partial z} + \frac{uv}{r} = -fu - \kappa v, \qquad (2')$$

$$\frac{1}{r}\frac{\partial}{\partial r}(ru) + \frac{\partial w}{\partial z} - Sw = 0, \qquad (4')$$

The above equations will be defined within a cylindrical domain

$$\Omega(r,\ \varphi,\ z) = [0,\ R_m] \times [0,\ 2\pi] \times [0,\ H_0]$$

with the following boundary conditions:

$$u_{r=Rm} = u_{r=0} = 0; \quad w_{z=0} = w_{z=H0} = 0;$$
$$v_{r=Rm} = v_{r=0} = 0; \quad \Phi_{r=Rm} = 0. \qquad (7)$$

It is worth pointing out that with time-dependent solution (6), the initial conditions for the other variables cannot be arbitrarily chosen because of the dynamical constraints of Equations (1′), (2′) and (4′), which will be demonstrated in section 5 to be of importance in constructing dynamically consistent 3D vortices for TC models. Unlike the numerical approach for which one can integrate a model with arbitrary initial conditions, that solution (6) contains a time-dependent factor puts a strong restriction on the allowed solutions for other variables. In other words, *given the vertical motion profile (6), the 3D structures and evolution of the PC can be estimated from Equations (1′), (2′), and (4′)*. This is opposite in philosophy to the previous quasi-balanced TC studies in which the PC has to be *a priori* assumed to estimate its associated SC (e.g. Eliassen, 1952; Willoughby, 1990b; Zhang and Kieu, 2006). Table I lists the definition and dimension of all the parameters used in the present study.

3. Analytical solutions

Since the ascending motion is assumed to occur only in the inner-core region (i.e. $r \le a$), the remaining solutions for variables u, v, and ϕ should be derived from Equations (1′), (2′) and (4′) for the inner-core region (I) and the outer region (II), separately.

3.1. Analytical solutions for region I

From the continuity equation (4′) and $w_1(r, z, t) = H(z)e^{\beta t}$, where $H(z) = W_0 \sin(\lambda z)$, the radial wind in region I is given by

$$u_1(r, z, t) = \left(SH - \frac{dH}{dz}\right) e^{\beta t}\frac{r}{2} + \frac{C_1}{r}$$
$$\equiv Qre^{\beta t} + \frac{C_1}{r}, \qquad (8)$$

Table I. Specification of parameters used for the present study.

Parameter	Definition	Value
a	Radius of the cloud disk or the RMW	100 km
β	Growth rate parameter	$10^{-6} - 10^{-5}$ s^{-1}
f	Coriolis parameter at 10°N	2×10^{-5} s^{-1}
H_0	Depth of the troposphere	20 km
H_{PBL}	Depth of the PBL	1 km
λ	Inversed depth of the troposphere ($= \pi/H_0$)	1.7×10^{-4} m^{-1}
κ_0	Frictional drag coefficient at $z = 0$	5×10^{-5} s^{-1}
R_{m}	Outer radius of a TC beyond which the ambient environment is at rest	2000 km
S	Stratification parameter ($\equiv N^2/g$)	10^{-5} m^{-1}

DOI: 10.1002/qj

where $Q(z) = W_0[S \quad \sin(\lambda z) - \lambda\cos(\lambda z)]/2$, and $C_1(z,t)$ vanishes after applying the boundary condition (6) at $r = 0$.

Plugging Equations (6) and (8) into Equation (2′), it is straightforward to obtain the following equation for the tangential wind in region I:

$$\frac{\partial v_1}{\partial t} + \left(Qr\frac{\partial v_1}{\partial r} + Qv_1 + H\frac{\partial v_1}{\partial z}\right)\mathrm{e}^{\beta t} = -fQ\mathrm{e}^{\beta t}r - \kappa v_1. \tag{9}$$

The only separable solution in radius that Equation (9) can admit is of the form: $v_1(r,z,t) = F_1(z,t)r$. Use of this form in Equation (9) gives

$$\frac{\partial F_1}{\partial t} = -\left(H\frac{\partial F_1}{\partial z} + 2QF_1 + fQ\right)\mathrm{e}^{\beta t} - \kappa F_1. \tag{10}$$

Consider a formal asymptotic expansion of the solution $F_1(z,t)$ in terms of the drag coefficient κ as follows:

$$F_1(z,t) = F^{(0)}(z,t) + \kappa(z)F^{(1)}(z,t) + \kappa^2(z)F^{(2)}(z,t) + O\{\kappa^3(z)\}. \tag{11}$$

Assuming that this series expansion converges at higher orders, we can obtain a solution for $F_1(z,t)$ with each order of $\kappa(z)$ after substituting (11) into (10). For the simplicity of our derivation, we only present the calculation up to the first-order correction.

Consider first the zero-order solution of Equation (10), which is governed by:

$$\frac{\partial F^{(0)}}{\partial t} = -\mathrm{e}^{\beta t}\left(H\frac{\partial F^{(0)}}{\partial z} + 2QF^{(0)} + fQ\right). \tag{12}$$

Let $F^{(0)}(z,t) = -f/2 + F_h(z,t)$, then

$$\frac{\partial F_h}{\partial t} = -\mathrm{e}^{\beta t}H\frac{\partial F_h}{\partial z} + 2QF_h. \tag{13}$$

A simple factoring technique suggests that the solution of (13) is of the form

$$F_h(z,t) = G(z)\exp(\mu\mathrm{e}^{\beta t}), \tag{14}$$

where μ is an arbitrary positive, dimensionless number. Plugging (14) into (13), followed by an integration, an explicit form for $F_h(z,t)$ could be derived as (see Appendix A)

$$F_h(z,t) = \frac{G_0\sin(\lambda z)\mathrm{e}^{-Sz}\exp(\mu\mathrm{e}^{\beta t})}{\left\{\tan\left(\frac{\lambda z}{2}\right)\right\}^{\frac{\mu\beta}{W_0\lambda}}}. \tag{15}$$

Thus, the zero-order solution for the tangential wind is given by

$$v_1^{(0)}(r,z,t) = r\left[\frac{G_0\sin(\lambda z)e^{-Sz}\exp(\mu\mathrm{e}^{\beta t})}{\left\{\tan\left(\frac{\lambda z}{2}\right)\right\}^{\frac{\mu\beta}{W_0\lambda}}} - \frac{f}{2}\right]. \tag{16}$$

where G_0 is an integration constant (with the unit of s^{-1}) that determines the initial strength of a vortex. Note that the double-exponential factor, $\exp(\mu e^{\beta t})$, is associated with the effects of the radial and vertical advection of angular momentum (Equations (13) and (14)) whereas the factor e^{-Sz} denotes the vertical weighting effects of the atmospheric stratification on ${v_1}^{(0)}$. Solution (16) contains an infinite number of possible solutions depending on the values of μ. However, the requirement of the regularity of (16) at $z = 0$ imposes a strong restriction on the range of μ. Specifically, by taking limit of (16), we have (Appendix A):

$$\frac{\mu\beta}{\lambda W_0} \le 1. \tag{17}$$

Given β, λ and W_0, the largest possible value of μ is: $\mu_{\max} = \lambda W_0/\beta$. In addition, by restricting the solutions only to the growing modes, the range of μ will be truncated to $\mu > 0$. To ease our subsequent discussion, let $\mu(\lambda, W_0) = 1 - \delta$, so that δ will be in the range of [0, 1], and so solution (16) can be rewritten as

$$v_1^{(0)}(r,z,t) = r\left[2G_0\sin^{\delta}\left(\frac{\lambda z}{2}\right)\cos^{2-\delta}\left(\frac{\lambda z}{2}\right)e^{-Sz} \times \exp\left\{\frac{W_0\lambda}{\beta}(1-\delta)e^{\beta t}\right\} - \frac{f}{2}\right]. \tag{18}$$

To help understand the physical implication of the parameter δ, Figure 3 shows the dependence of the vertical profile of ${v_1}^{(0)}(r,z,t)$ on δ at $r = a$. First, the zero-order solution exhibits a deep layer of cyclonic flow in the troposphere, with the peak tangential wind shifting from the surface to midlevel as δ increases from 0 to 1. Second, solution (18) shows the strong dependence of growth rate on the vertical structure of tangential wind. Indeed, if the e-folding time (τ_e) is defined from the exponent in (18) as

$$\tau_{\mathrm{e}} = \frac{1}{\beta}\ln\left\{\frac{\beta}{W_0\lambda(1-\delta)}\right\},$$

we can see that the higher level the peak tangential flow (i.e. the larger δ) is located, the slower rate the TC vortex will grow (i.e. the larger τ_{e}). In other words, *a TC vortex with the peak tangential wind near the surface will amplify faster than one located higher up*. This is a result of the absolute angular momentum conservation (Zhang *et al.*, 2001). That is, it would take a much shorter time for the SC to spin up a TC vortex through its radial and vertical advection of the absolute angular momentum if the peak rotational flow is located in the lowest inflow layer than in that above. Because the zero-order solution applies to frictionless vortices, $\delta = 0$ gives rise to tangential winds peaked at the surface, and meanwhile results in the fastest growth of the surface wind (Figure 3). Note that the e-folding time also depends on the depth of the troposphere (through λ), the mean vertical motion W_0, and static stability (through β). Because the maximum tangential wind in rapidly intensifying TCs is often observed near the top of the

DOI: 10.1002/qj

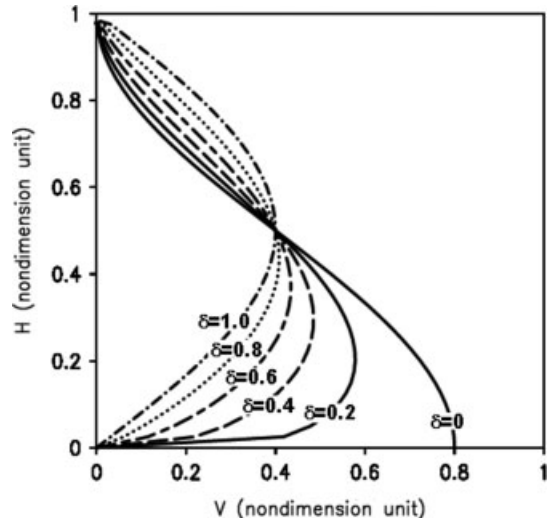

Figure 3. Vertical profiles of the tangential winds at the zero order, $v^{(0)}{}_1$(z,a,0), given by Equation (18), with different values of δ. They are plotted with non-dimensional units.

PBL, it is desirable to take into account the next order of the frictional correction, as discussed below.

Use of (11) and (18) in Equation (10), the first-order frictional correction $F^{(1)}(z,t)$ is governed by

$$\frac{\partial F^{(1)}}{\partial t} = -\mathrm{e}^{\beta t}\left(H\frac{\partial F^{(1)}}{\partial z} + 2QF^{(1)}\right) - F^{(0)}. \qquad (19)$$

Following the same procedures as that for the zero order, and noting that $F^{(0)}(z,t) = -f/2 + F_h(z,t)$, the solution for $F^{(1)}(z,t)$ can be approximated as

$$F^{(1)}(z,t) = \frac{2G_1W_0\lambda}{\beta}\cos^2\left(\frac{\lambda z}{2}\right)\mathrm{e}^{-Sz} \times \frac{\exp(W_0\lambda \mathrm{e}^{\beta t}/\beta) - \tan(\lambda z/2)}{W_0\lambda \mathrm{e}^{\beta t}/\beta - \ln[\tan(\lambda z/2)]}, \qquad (20)$$

where G_1 is an integration constant to be determined later. Note that only the most weighted (i.e. lower-order) contribution to $F^{(1)}(z,t)$ is included in (20) (see Appendix II).

With the first-order frictional correction, the tangential wind in region I is now given by:

$$v_1(r,z,t) = [F^{(0)}(z,t) + \kappa(z)F^{(1)}(z,t)]r \equiv K(z,t)r, \qquad (21)$$

where $K(z,t)$ is defined by

$$K(z,t) = -\frac{f}{2} + 2G_0\cos^2\left(\frac{\lambda z}{2}\right)\mathrm{e}^{-Sz} \times \left[\exp\left(\frac{W_0\lambda}{\beta}e^{\beta t}\right) + \varepsilon\frac{\exp(W_0\lambda \mathrm{e}^{\beta t}/\beta) - \tan(\lambda z/2)}{W_0\lambda \mathrm{e}^{\beta t}/\beta - \ln[\tan(\lambda z/2)]}\right], \qquad (22)$$

and $\varepsilon = \kappa W_0\lambda G_1/\beta G_0$. Figure 4 shows the vertical profiles of the zero-order solution (18) with $\delta = 0$, the first-order frictional correction (20) and the total solution (21) at four different instants of time. Obviously, the surface friction reduces the surface wind to near null, causing the peak wind to be located above the PBL (Figure 4(b)). In general, the larger the κ, the higher level the peak of the frictional correction will be located. Of interest is that because the zero-order solution increases rapidly with time, and the level of its peak magnitude shifts slightly downwards; similarly for the total tangential winds (Figure 4(c)). In terms of the growth rate, however, *the TC vortex tends to grow from the bottom upwards due to the fastest growth at the surface due to the zero-order solution*. This result appears to provide an important theoretical insight into the dynamical behaviours of growing vortices during the tropical cyclogenesis stage. Namely, the TC vortex tends to spin up from the bottom upwards as a result of the inward advection of the absolute angular momentum in the lowest inflow layer (Zhang and Bao, 1996; Hendricks *et al.*, 2004; Montgomery *et al.*, 2006; Kieu and Zhang, 2008).

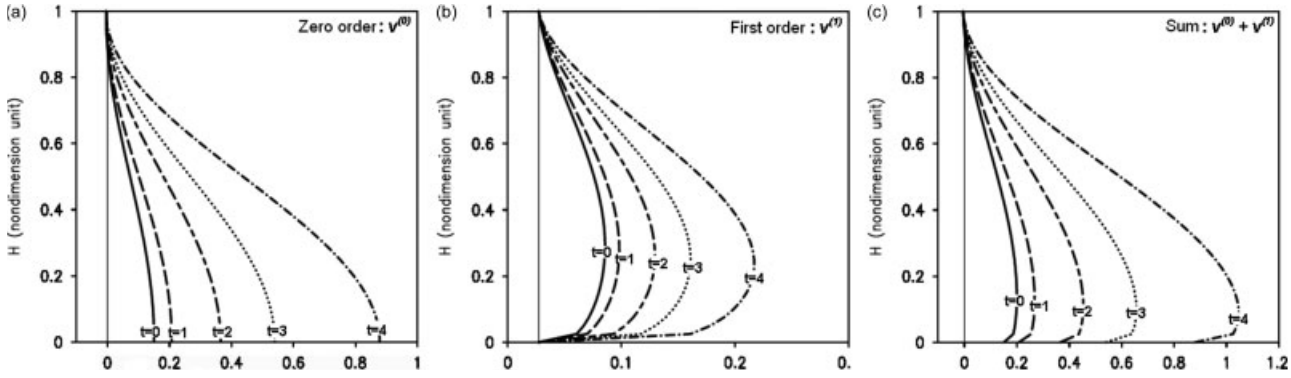

Figure 4. Vertical profiles of the mean tangential wind in region I at times $t = 0$, 1, 2, 3, 4 for (a) the zero-order $v^{(0)}{}_1$(z,a,t) given by Equation (18); (b) the first-order frictional correction $v^{(1)}{}_1$(z,a,t) given by Equation (20); and (c) the sum of the zero- and first-order solutions given by Equation (21). Note that $\delta = 0$ is required for the zero-order solution, and that all the parameters have been non-dimensionalized.

DOI: 10.1002/qj

To find $\phi_1(r, z, t)$ in region I, substituting solutions for v_1, w_1, and u_1 into Equation (1′), after some manipulations, gives

$$\frac{\partial \phi_1}{\partial r} = -r(Q\beta e^{\beta t} + Q^2 e^{2\beta t} + He^{2\beta t}\frac{dQ}{dz} - K^2 - fK - Q\kappa). \quad (23)$$

A simple integration of (23) with respect to r leads to

$$\phi_1(r, z, t) = \Phi_a - \frac{(a^2 - r^2)}{2}\left(K^2 + fK - Q\beta e^{\beta t} - Q\kappa - Q^2 e^{2\beta t} - He^{2\beta t}\frac{dQ}{dz}\right), \quad (24)$$

where $\Phi_a(z)$ is the geopotential height perturbation at $r = a$, and it will be determined later with the geopotential height distribution in region II.

3.2. Analytical solutions for region II

Exact solutions for region II can be derived using the same procedures as those for region I. First, integrating the continuity equation (4′), with $w_2(r, z, t) = 0$, gives

$$u_2(r, z, t) = C_1(z, t) - \frac{C_2(z, t)}{r}, \quad (25)$$

where $C_1(z, t)$ and $C_2(z, t)$ are integral functions. Using Equation (4) at $r = a$ and the boundary condition (6) yields

$$C_1 = 0 \text{ and } C_2 = \frac{a^2}{2}\left(\frac{dH}{dz} - SH\right)e^{\beta t}.$$

So, the solution for the radial wind in region II is

$$u_2(r, z, t) = -\frac{1}{2}\left(\frac{dH}{dz} - SH\right)e^{\beta t}\frac{a^2}{r} \equiv e^{\beta t}\frac{a^2 Q}{r}. \quad (26)$$

Substitution of u_2 into Equation (2′), followed by some simple rearrangements, yields

$$\frac{\partial v_2}{\partial t} = -a^2 e^{\beta t}\left(\frac{Q}{r}\frac{\partial v_2}{\partial r} + \frac{Q}{r^2}v_2 + f\frac{Q}{r}\right) - \kappa v_2. \quad (27)$$

The only separable solution of (27) is of the form of $v_2(r, z, t) = F_2(z, t)/r$, so we have

$$\frac{\partial F_2}{\partial t} = -e^{\beta t}a^2 fQ - \kappa F_2. \quad (28)$$

Integrating it gives an explicit solution for the tangential wind in region II:

$$v_2(r, z, t) = \frac{1}{r}\left(\frac{-e^{\beta t}Qfa^2}{\beta + \kappa} + Ze^{-\kappa t}\right), \quad (29)$$

where $Z(z)$ is an integral function of z, and it can be determined by matching $v_1(r, z, t)$ and $v_2(r, z, t)$ at $r = a$ and $t = 0$ as follows

$$Z(z) = \left(K + \frac{Qf}{\beta + \kappa}\right)a^2. \quad (30)$$

By plugging u_2, v_2, w_2 into Equation (1′), we obtain

$$\frac{\partial \phi_2}{\partial r} = -\left(e^{\beta t}Qa^2\frac{\beta + \kappa}{r} - e^{2\beta t}\frac{Q^2 a^4}{r^3} - \frac{C^2}{r^3} - \frac{fC}{r}\right), \quad (31)$$

where $C(z, t) = \left(\frac{-e^{\beta t}Qfa^2}{\beta + \kappa} + Ze^{-\kappa t}\right)$.

Finally, integrating (31) gives the geopotential height perturbation in region II:

$$\phi_2(r, z, t) = \Phi_0 + \{e^{\beta t}a^2 Q(\beta + \kappa) - fC\}\ln\frac{R_m}{r} - e^{2\beta t}\frac{a^4 Q^2}{2r^2} - \frac{C^2}{2r^2}, \quad (32)$$

where radius R_m and $\Phi_0(z, t)$ are defined such that $\phi_2|_{r=Rm} = 0$. All the solutions for the wind and mass fields in both region I and II are thus derived completely.

One should keep in mind that the analytical solutions obtained above are suitable only for the intensifying stage during which the energy supply is assumed to be favourable for the full intensification of TCs with little environmental influences. As the storms reach their maximum intensity, the exponential growth of the vertical motion as assumed in (6) is no longer valid, so the time-dependent solutions cannot be further extended in time. Meanwhile, there must be an upper limit for the mean upward motion, which may be closely related to the MPI (Emanuel, 1986; Holland, 1997). Thus, we have to restrict the validity of the above growing solutions to a range of [0, T_m], where T_m is the shortest time at which the maximum intensity is reached.

4. Verification

In this section, we validate the above analytical solutions against some well-documented observations and model simulations in the literature (e.g. McBride, 1981; McBride and Zehr, 1981; Willoughby *et al.*, 1982; Willoughby, 1990a; Liu *et al.*, 1999). Some important features may be summarized as follows:

i The TC flow is cyclonic prevalently throughout the troposphere and it becomes anticyclonic only in a thin layer near the tropopause;
ii the tangential wind increases near-linearly with radius until reaching the RMW and then decreases slowly to the ambient value at a very large distance;
iii the tangential wind is peaked near the top of the PBL and then decreases with height, especially near the RMW; and

DOI: 10.1002/qj

iv the rotational flow in the inner-core region grows much faster than that in the outer region.

Some other typical features may include:

v radial inflow and outflow at the low and upper levels, respectively;
vi the peak vertical motion in the mid-troposphere with a null value at the surface and the tropopause; and
vii lower pressures (or geopotential heights) in the core region throughout the troposphere except in the upper layer where the horizontal winds become anticyclonic.

In the next section, let us see to what extent the analytical solutions obtained in section 3 could reproduce the above-mentioned features.

4.1. Growth rates

A comparison of solutions (21) and (29) show clearly that the tangential wind in the inner-core region $v_1(r, z, t)$ grows at a rate much faster (due to the double exponential factor) than that in the outer region $v_2(r, z, t)$, as listed at (iv). Figure 5 shows an example of hurricane *Diana* (1984); Willoughby (1990a,b) provides more TC cases. Evidently, the tangential wind within the RMW nearly doubles in magnitude in 24 hours whereas its outer-region magnitude exhibits a slow increase. Our solutions capture well this drastic difference in the growth rate between the inner-core and outer regions.

A further examination of the growth rates shows that the spin-up of the PC is more complicated than that of the SC. Namely, the PC exhibits a rapid amplification rate in the core region and a slower rate outside, whereas the SC grows just exponentially in both the inner and outer regions. This implies the distinctive dynamics between the rotational flows and SCs during TC growth. Physically, this intriguing PC behaviour in the inner-core region could be attributed to the radial-inward and upward advection of the absolute angular momentum. That is, the axisymmetry of TCs requires both the radial and tangential winds to vanish at the vortex centre and in the far outer region. This implies that the tangential wind has to attain its maximum value somewhere near the core of the vortex (i.e. $r = a$ in our model). It follows that the radial inward advection in the PBL will help accelerate (decelerate) the PC in the inner-core (outer) region. In addition, the ascending motion in the inner-core region advects larger angular momentum upwards, facilitating further the amplification of the TC vortex in the layers above. Thus, the dynamical impacts of the SC on the PC are of vital importance in determining the growth of TCs.

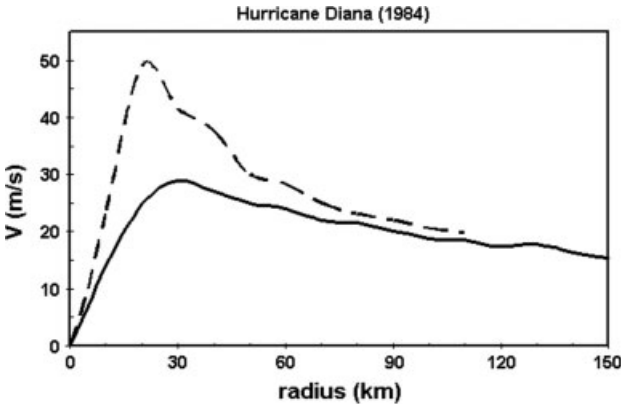

Figure 5. Growth of the 850 hPa tangential wind in hurricane *Diana* (1984) valid during the periods 2335 UTC on 9 September to 1514 UTC on 10 September (solid), and 0228 to 0903 UTC on 11 September 1984 (dashed). (Reproduced from Willoughby, 1990.)

Now let us attempt to validate our time-dependent solutions with the cloud-resolving simulation of hurricane *Wilma* (2005). We take $W_0 = 0.12$ m s^{-1}, obtained by averaging the simulated vertical motion over an area with $r = 400$ km from the eye centre at 6 hours into the integration, and use the maximum tangential wind of 30 m s^{-1} at $z = 1.6$ km. To represent the damping effects of the PBL, we use the drag coefficients of the form

$$\kappa(z) = \kappa_0 \exp[-(z/H_{\mathrm{PBL}})^2],$$

where $\kappa_0 = 2.5 \times 10^{-5}$ s^{-1}. This $\kappa(z)$ profile corresponds to a near-constant drag coefficient in the PBL with a depth of H_{PBL} and then it decreases rapidly upwards. With the above inputs and some other parameters given in Table I, iterations of solution (21) through trial and error give $G_0 = 6.6 \times 10^{-9}$ s^{-1} and $\varepsilon = 0.25$. To facilitate the comparison with model simulations, we provide here an analytical expression for the surface central pressure drop $\delta p_{\min}$, which can be derived readily by setting $r = 0$ in Equation (24) to give $\phi_{\min}$. Since $\delta p_{\min} = \rho \phi_{\min}$, we have:

$$\delta p_{\min}(t) = \rho \Phi_a - \frac{\rho a^2}{8}(4K^2_{|z=0} + 4fK_{|z=0} + 2W_0\lambda\beta e^{\beta t} + 2W_0\lambda\kappa - (W_0\lambda)^2 e^{2\beta t}), \quad (33)$$

where Φ_a is evaluated from solution (32) by setting $r = a$, i.e. $\Phi_a = \phi_2(r = a, z = 0, t)$, and

$$K_{|z=0} = 2G_0 \exp\left(\frac{W_0\lambda}{\beta} e^{\beta t}\right) - \frac{f}{2}.$$

Figure 6 compares the time evolution of V_{MAX} and $\delta p_{\min}$ associated with hurricane *Wilma* (2005) between the theory and WRF prediction, using the previously estimated value of $\beta = 2 \times 10^{-6}$ s^{-1}. One can see that the theory-predicted growth of $\delta p_{\min}$ fits well the WRF-predicted growth, i.e. showing a slow growth of the TC intensity at first and more rapid deepening at later times. In particular, the maximum theoretical rate of surface pressure drop is about 10 hPa hr^{-1}, which is comparable to the observed 9 hPa hr^{-1} rate. An examination of the simulation results shows the presence of very weak vertical wind shear during this deepening period, which explains why the exact solution could capture well the observed pressure drop. However, the exact solution begins to overpredict the maximum

DOI: 10.1002/qj

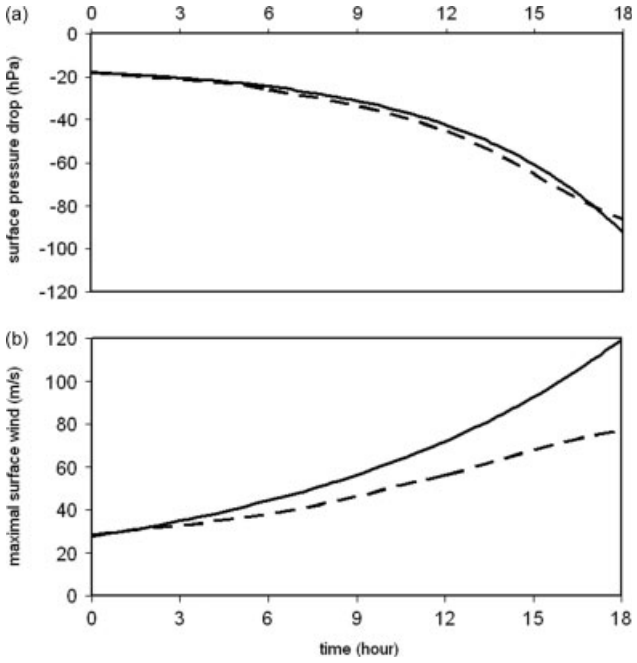

Figure 6. Comparison of the time series of the exact solutions (33) and (21) (solid) with the 36-hour WRF model simulation (dashed) of hurricane *Wilma* (2005) for (a) the surface central pressure drop (hPa), and (b) the axisymmetric component of the maximum tangential wind (m s^{-1}), for the period 1200 UTC on 18 October to 0600 UTC on 19 October 2005 (also see Figure 1(a)).

wind more after a couple of hours. This appears to be a consequence of the use of the first-order frictional parametrization in the PBL, whose effects are often treated as being proportional to the squared surface wind (Zhang *et al.*, 1999). Despite this discrepancy, the result reveals that such rapid intensification is depicted well by the double exponential growth associated with the nonlinear terms in the primitive equations. It follows that the rapid deepening of most TCs could be attributed to the nonlinear dynamical processes associated with the SC. In nature, the TC growth is often offset by vertical wind shear, horizontal deformation, dry intrusion, and friction. So, our theoretical e-folding time should be considered as an upper bound for the growth of TCs during their rapid intensification stage.

One may note that the RMW in the exact solutions does not vary with time due to the use of a top-hat forcing function within a fixed radius (i.e. $r \leq a$ in Equation (6)), whereas both the observations and simulations document a gradual contraction of the RMW during TC intensification (e.g. Willoughby *et al.*, 1982; Liu *et al.*, 1999). However, the analytical result, in which the tangential flow in the inner-core region intensifies at a rate much faster than that in the outer region, is a good indication of the collapse of the RMW, as also discussed by Schubert and Hack (1982). Of course, with the RMW fixed as in our model, some discontinuities of the tangential flows will develop with time at $r = a$, as can be seen from solutions (21) and (29). Our initial attempts using a Gaussian function for solution (6) can eliminate such discontinuities and still capture the behaviours of tangential flows that are similar to those with the top-hat profile, at least in the asymptotic limit at the small- and large-radius approximation. The use of such a smooth function will also allow for the contraction of the RMW. This will be presented in one of our forthcoming papers.

4.2. The 3D flow structures

Solutions (21) and (29) show that the tangential wind increases linearly with radius for $r \leq a$ and decreases inversely with radius for $r > a$. This radial distribution fits well the familiar pictures of TCs even at the early stage (e.g. Willoughby, 1990), as listed at (ii). More notably, the two solutions show cyclonic flows in a deep layer in the troposphere and anticyclonic flows in a thin layer beneath the tropopause, as listed at (i). Figure 7 compares the vertical profile of the area-averaged tangential flow over the inner-core area as given by (21) with $W_0 = 0.12$ m s^{-1}, $G_0 = 5.4 \times 10^{-9}$ and $\varepsilon = 0.25$ to the observed by McBride (1981), where G_0 and ε are iteratively estimated in the same way as previously mentioned, but based on the observed maximum wind and its corresponding altitude. Except for the slope of the theoretical tangential wind profile that is steeper than the observed, the analytical solution shows a general consistency with a dominant cyclonic flow in the troposphere and a peak near the top of the PBL due to the inclusion of frictional effects. The physical reasoning for such a deep layer of cyclonic flow is again attributable to the roles of the SC in transporting the absolute angular momentum. Solutions (6), (8) and (26) also provide a consistent description of the SC with an inflow in the lower half and an outflow in the upper half of the troposphere, and the maximum vertical motion at the middle level (Figure 8), as listed at (v) and (vi). The atmospheric stratification

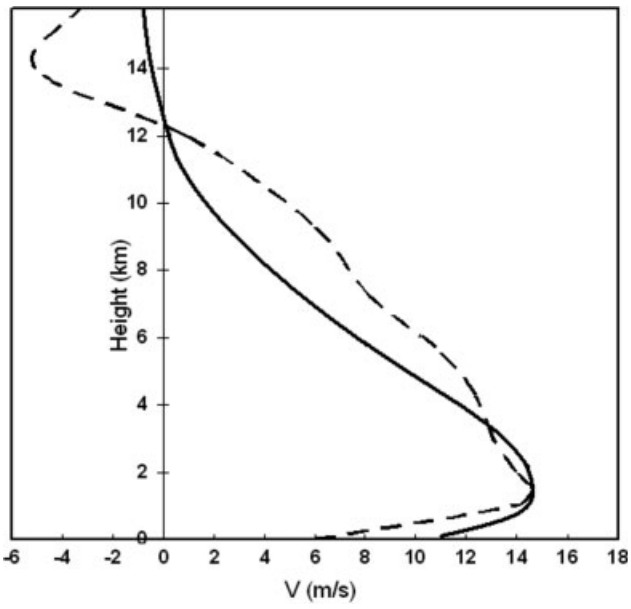

Figure 7. Comparison of the vertical profile of the mean tangential wind estimated from Equation (21) (solid) with that observed in West Pacific typhoons (dashed). The observed profile is reproduced from McBride (1981).

DOI: 10.1002/qj

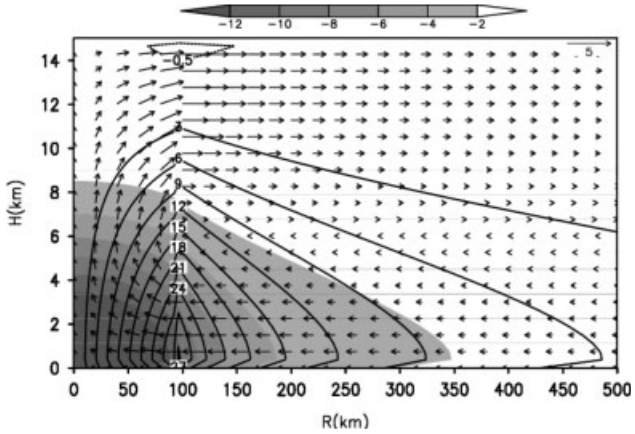

Figure 8. Radius–height cross-section of the tangential wind (contours at 3 m s^{-1} intervals) and pressure perturbations (shading at 2 hPa intervals), superimposed with in-plane flow vectors, as constructed from the analytical solutions obtained in section 3.

makes the inflow layer somewhat shallower than the outflow layer in the pseudo-height vertical coordinate.

4.3. The 3D mass field

The observed bow shape of the geopotential height, listed at (vii), can be reproduced by solutions (24) and (32). To see this, we consider each half of the troposphere separately. Because $Q \approx -\,\mathrm{d}H/\mathrm{d}z$ is negative and $\mathrm{d}Q/\mathrm{d}z \approx -\,\mathrm{d}^2H/\mathrm{d}z^2$ is positive in the lower atmosphere, the first four (last two) terms inside the parenthesis of (24) will contribute positively (negatively) to the decrease of geopotential height at each level. Since $K(z,t)$ is a sensitive function of time (i.e. due to the double exponential factor), the first two terms containing K will become more dominant with time, and lower pressures are guaranteed to develop in the inner-core region after a while. In the upper half of the troposphere, because $Q > 0$ and $\mathrm{d}Q/\mathrm{d}z < 0$, the positive contributions of the first two terms, though decreasing with height, will be compensated by the negative contributions of the last four terms in the parenthesis of (24). Due to the dominant time-dependence of $K(z,t)$, we may still expect to have lower pressures developed in the upper troposphere with time and this explains the development of a deep layer of low pressure in the troposphere. Near the tropopause, however, K becomes very small due to the strong dependence on height (cf. Figure 7 and Equation (24)) so that a weak high-pressure system may be seen corresponding to anticyclonic flows aloft.

4.4. Gradient-wind approximation

Since the gradient-wind approximation has been widely accepted in previous TC studies, particularly in relation to the balance theory (e.g. Willoughby, 1990b, Zhang *et al.*, 2001), it is of interest to see how well this balance relation is represented in our analytical solutions. This can be done simply by deriving the geopotential height perturbation from the gradient wind balance, i.e.

$$-\frac{v^2}{r} = -\frac{\partial \phi_b}{\partial r} + fv, \tag{34}$$

and then comparing it with solutions (24) and (32). Substituting tangential wind $v_1(r,z,t)$ and $v_2(r,z,t)$ into Equation (34) will yield ϕ_b for region I and II, separately. For example, a comparison of the balanced geopotential height ϕ_b with solution (24) for region I gives

$$\left|\frac{\phi_1-\phi_\mathrm{b}}{\phi_1}\right| \cong \left|\frac{\phi_1-\phi_\mathrm{b}}{\phi_1}\right|_{t=0} \times \left[\frac{\cos(\lambda z)}{\cos^2(\lambda z/2)}\,\frac{\mathrm{e}^{2\beta t}}{\exp(W_0\beta \mathrm{e}^{\beta t}/\lambda)}\right]^2. \tag{35}$$

Equation (35) shows that, no matter how large the difference between the exact solution and the gradient-wind approximation at the initial time is, the relative difference will approach zero as the denominator increases rapidly with time. Therefore, the gradient wind balance is expected to be a better approximation at the later stages. The gradient balance relation should be more easily satisfied in the outer region. Note that, similar to the quasi-balanced theory for which the radial wind is derived from the Sawyer–Eliassen equation and the gradient wind approximation (34) is used as a constraint between the mass and the wind field, the radial wind in our model is diagnosed from the continuity equation, given an explicit solution for the vertical motion (6). The radial momentum equation (1′) will therefore serve as a constraint on the mass and wind fields. With the wind fields given by solutions (6), (8), and (21) in the inner-core region, the mass field has to be determined accordingly to satisfy Equation (1′).

5. Applications

Much of our current understanding of TCs is based mainly on the modelling studies of both idealized hurricane-like vortices and real TC cases (e.g. Ooyama, 1969; Willoughby, 1979; Rotunno and Emanuel, 1987; Liu *at el.*, 1997; Wang and Holland, 1996; Zhu *et al.*, 2001; Montgomery *et al.*, 2006). In these modelling studies, it is necessary to either initialize the TC models with axisymmetrical vortices or enhance the initial TC vortices via the use of vortex-bogussing techniques (Kurihara *et al.*, 1993; Wang, 1998; Xiao *et al.*, 2000; Pu and Braun, 2001; Wang *et al.*, 2008). Even though the current global models have become fine enough to capture a sizeable percentage of TC development, vortex bogussing still appears to be of critical importance in the forecasts of both TC track and intensity, even in relatively data-rich areas (Heming, 2008).

Except for the assimilation of real observations, the vortex bogussing requires an *ad hoc* specification of vertical structures (Kurihara *et al.*, 1993; Wang, 1998; Heming and Radford, 1998; Xiao *et al.*, 2000; Wang *et al.*, 2008).

DOI: 10.1002/qj

In addition, in many cases only the PCs could be initialized, and the pertinent SCs have to rely on the TC models to spin up. Our exact solutions indicate that the vertical structures of tangential winds at the model initial time could produce significant impact on the subsequent intensity changes of TCs, as mentioned before. This is consistent with some sensitivity experiments reported by Wang (1998), who showed strong dependence of TC movement and intensity changes on the vertical profiles of the initial tangential flows.

In this section, we shall show how our analytical solutions could be used to construct TC-like vortices for initialization of hurricane models. All one has to do is to set $t = 0$ in solutions (6), (8), (21), (24), (26), (29), and (32), which will yield the 3D fields of w, u, v, and ϕ in both region I and II. As indicated by Equations (1′), (2′), and (4′), our solutions provide complete and dynamically consistent 3D distributions for both the PC and SC. Specifically, the tangential wind at $t = 0$ is given by

$$v_1(r, z, 0) = K(z, 0)r \qquad \text{for } r \le a, \qquad (21')$$

$$v_2(r, z, 0) = \frac{1}{r}\left(\frac{-Qfa^2}{\beta} + Z\right) \quad \text{for } r > a. \qquad (29')$$

The geopotential height perturbation is given by

$$\phi_1(r, z, 0) = \Phi_a - \frac{(a^2 - r^2)}{2}\left(K^2 + fK - Q\beta - Q^2 - H\frac{\mathrm{d}Q}{\mathrm{d}z}\right) \qquad \text{for } r \le a, \qquad (24')$$

$$\phi_2(r, z, 0) = \Phi_0 + a^2 Q(\beta + \kappa - fC)\ln\frac{R_m}{r} - \frac{a^4Q^2}{2r^2} - \frac{C^2}{2r^2} \qquad \text{for } r > a, \qquad (32')$$

where $C(z) = Qfa^2/(\beta + \kappa) + Z$, $\Phi_0(z) = (a^4Q^2 + C^2)/R_m^2$, and $\Phi_a(z) = \phi_2(a, z, 0)$. The radial wind is given by

$$u_1(r, z, 0) = Qr \qquad \text{for } r \le a, \qquad (8')$$

$$u_2(r, z, 0) = a^2Q/r \qquad \text{for } r > a. \qquad (26')$$

The vertical motion is given by

$$w_1(r, z, 0) = W_0 \sin(\lambda z), \qquad \text{for } r \le a, \qquad (6a')$$

$$w_2(r, z, 0) = 0 \qquad \text{for } r > a. \qquad (6b')$$

The above 3D vortex structures appear at first to contain too many free parameters (e.g. β, λ, κ_0, W_0, R_m, S). However, most of the parameters are nearly constants and suitable for all of the TCs (Table I). The only initial inputs we need for the above solutions are the area-averaged maximum vertical motion (W_0), RMW (a), the Coriolis parameter (f), and the frictional correction (ε). In practice, W_0 could be approximately evaluated from a diabatic heating rate profile through Equation (5), assuming a balance between adiabatic cooling and diabatic heating. Such a heating profile seems to be feasible with today's observing platforms. Specifically, satellite retrieval algorithms, based on precipitation-rate profile retrievals, have recently been developed to estimate the vertical distribution of latent heating in TCs using Special Sensor Microwave Imager (SSM/I) and Tropical Rainfall Measuring Mission (TRMM) microwave imager measurements (e.g. Rodgers *et al.*, 1998; Tao *et al.*, 2006). With a numerical approach, Zhu *et al.* (2002) developed an algorithm to initialize TC vortices using the temperature (or heating) profiles retrieved from the Advanced Microwave Sounding Unit (AMSU-A) data. Parameters G_0 and ε can be calculated from (21′) in the same way as that described in section 4, using an observed maximum tangential wind at its corresponding altitude.

Figure 8 shows an example of a TC vortex using the parameters given in Table I, $W_0 = 0.12$ m s^{-1}, $G_0 = 5.4 \times 10^{-9}$ s^{-1}, and $\varepsilon = 0.2$; the latter two parameters are evaluated from Equation (21′) with a hypothetical maximum tangential wind of 30 m s^{-1} at $z = 1$ km, and $a = 100$ km. It is apparent that, except for small sharp changes at $r = a$ due to the first-order matching of Equation (30), the TC flow structures are reasonably constructed with the cyclonic winds decreasing upwards and outwards. The same procedures may be used to construct the 3D flow fields for a mature hurricane with intense diabatic heating in the eyewall.

6. Concluding remarks

In this study, the dynamical processes leading to the rapid intensification of TCs are examined with an analytical model, in which the nonlinear terms in the horizontal momentum equations are attained. An important procedure in this analytical model is to bypass the sophisticated moist thermodynamical processes by assuming a time-dependent solution for the vertical motion with a given growth rate in the core region. Our approach, deriving the TC intensity from the vertical motion (or heating function), differs radically from the previous quasi-balanced studies in which the rotational flows have to be *a priori* assumed in order to estimate their associated secondary circulations.

The exact solutions so obtained are shown to capture well many fundamental dynamics of TCs and their rapid intensifications. Specifically, the solutions for the rotational flows exhibit double-exponential growth in the inner-core region, as compared with their much slower growth in the outer region, which to our knowledge has not been previously shown. The central pressure drops could occur at the squared double-exponential rates. In particular, our analytical solutions show drastically different growth rates between the PC and SC, i.e. with a much faster spin-up rate of the rotational flows and deepening rate of the surface pressure than that of the SC due to the nonlinear advection effects in the horizontal momentum equations. This indicates that the TC intensification from the linear growth of the SC, as shown in the previous studies, tends to be underestimated in magnitude and oversimplified by neglecting the nonlinear terms.

DOI: 10.1002/qj

Results reveal further that the levels of the peak tangential flows shift downwards as TCs intensify, and that the lower the levels, the faster the TCs will grow under the absolute angular momentum conservation. These results have important implications for the initialization of TC models with bogussed vortices, because both the magnitude and level of the peak tangential winds affect the forecasts of subsequent intensity and intensity changes.

The analytical solutions obtained herein are shown to be also useful for initializing TC models when the mean diabatic heating or vertical motion could be approximated by top-hat profiles. Only a few initial inputs need to be specified from observations. An important difference from the previous bogussing technique is that our vortex initialization does not require *a prior* specification of the vertical structure of the rotational flows. Although the use of the top-hat function causes some discontinuities of solutions at $r = a$, it should be noted that our results associated with either the growth rates or the vertical structures of the PCs and SCs remain valid even when a smoother profile of the vertical motion, e.g. the Gaussian profile, is employed. In fact, the discontinuities only affect the vortex structure near $r = a$, and they can be effectively reduced by using a continuous step function.

In a forthcoming article, we will study further the growth and structures of TCs with different vertical motion functions, instead of the top-hat radial profile, and validate the exact solutions using more real-data and model-simulated TC cases.

Acknowledgements

We would like to thank Drs. Ferd Baer and Eitan Tadmor for helpful discussions, Dr. Mike Montgomery and an anonymous reviewer for their critical review of this manuscript, and to Ms. H. Chen for allowing us to use her simulated hurricane *Wilma* (2005) data. This work was supported by NSF grant ATM-0758609, NASA grant NNG05GR32G, and ONR grant N000140710186. The first author was also partly funded by Vietnam Education Foundation Fellowship.

Appendix A

Derivation of Solution (15)

To obtain Equation (15), substituting Equation (12) into Equation (11) and manipulating for a few steps, a differential equation for *G(z)* is obtained:

$$\frac{\mathrm{d}G}{G} = \frac{W_0\lambda\cos(\lambda z) - W_0 S\ \sin(\lambda z) - \mu\beta}{W_0\sin(\lambda z)}\mathrm{d}z. \tag{A.1}$$

Integrating (A.1) with respect to z gives:

$$\ln(G) = \ln[\sin(\lambda z)] - \frac{\mu\beta}{W_0\lambda}\ln\left\{\tan\left(\frac{\lambda z}{2}\right)\right\} + \ln(G_0) - Sz, \tag{A.2}$$

from which Equation (13) is followed readily as

$$G(z) = \frac{G_0\sin(\lambda z)\mathrm{e}^{-Sz}}{\left\{\tan\left(\frac{\lambda z}{2}\right)\right\}^{\frac{\mu\beta}{W_0\lambda}}}. \tag{A.3}$$

Note at $z = 0$, *G(z)* may be singular. To eliminate this singularity, there must be some restriction on λ,β,μ, and W_0. Using L'Hôpital's rule, one will obtain the criterion (17), i.e. $\mu\beta < \lambda W_0$.

Appendix B

Derivation of Solution (20)

Let $F^{(1)}(z, t) = \Gamma(z, t)F_h(z, t)$, from Equations (10)–(11), we have

$$F_h\frac{\partial\Gamma}{\partial t} = -\mathrm{e}^{\beta t}\ HF_h\frac{\partial\Gamma}{\partial z} - F^{(0)}, \tag{B.1}$$

or

$$\mathrm{e}^{-\beta t}\frac{\partial\Gamma}{\partial t} + H\frac{\partial\Gamma}{\partial z} = -\frac{F^{(0)}\mathrm{e}^{-\beta t}}{F_h}. \tag{B.2}$$

After performing coordinate transformation from (z, t) to a pair of new dependent variables (p, q) defined by

$$p = \int \mathrm{e}^{\beta\tau}\mathrm{d}\tau = \frac{1}{\beta}\mathrm{e}^{\beta t} \quad \text{and}$$
$$q = \int \frac{1}{H(\tau)}\mathrm{d}\tau = \frac{1}{\lambda W_o}\ln\left\{\tan\left(\frac{\lambda z}{2}\right)\right\}, \tag{B.3}$$

Equation (B.2) can be rewritten as

$$\frac{\partial\Gamma}{\partial p} + \frac{\partial\Gamma}{\partial q} = R(p, q) \equiv -\frac{F^{(0)}(p, q)\mathrm{e}^{-\beta t(p)}}{F_h(p, q)}, \tag{B.4}$$

where

$$F_h(p, q) = \frac{\sin(\lambda z)e^{-S\ z}\exp(\mu e^{\beta\ t})}{\left\{\tan\left(\frac{\lambda z}{2}\right)\right\}^{\frac{\mu\beta}{W_0\lambda}}}, \tag{B.5}$$

where the implicit dependence of z on q and t on p will be obtained from (B.3). The solution of (B.4) can be found by first finding its homogeneous solution, and then using the method of variational coefficients (e.g. Polyamin *et al.*, 2001), we obtain

$$\Gamma(p, q) = \int_{p_0}^{p} R(\tau, q - p - \tau)\mathrm{d}\tau + G(p - q) = \int_{p_0}^{p} \frac{F^{(0)}(\tau, q - p - \tau)\mathrm{e}^{-\beta t}}{F_h(\tau, q - p - \tau)}\mathrm{d}\tau + G(p - q), \tag{B.6}$$

DOI: 10.1002/qj

where $G(p-q)$ denotes a function of $(p-q)$. To eliminate the singularity of $q(z)$ at $z=0$,

$$G(p-q) = G\left\{\left(\frac{e^{\beta r}}{\beta}\right) - \frac{\ln\{\tan(\lambda z/2)\}}{\lambda W_0}\right\}$$

will be chosen as a constant G_1. Then, solution for (B.4) is given by

$$F^{(1)}(z,t) = \int_0^{\mu_{\max}} \left[\left\{G_1 + \int_{p_0}^{p} \frac{F^{(0)}(\tau, q-p-\tau)e^{-\beta t}}{F_h(\tau, q-p-\tau)}\mathrm{d}\tau\right\} \times \frac{\sin(\lambda z)\mathrm{e}^{-S\,z}}{\left\{\tan\left(\frac{\lambda z}{2}\right)\right\}^{\frac{\mu\beta}{W_0\lambda}}} \exp(\mu \mathrm{e}^{\beta t})\right] \mathrm{d}\mu. \tag{B.7}$$

Note that the term G_1 is the most weighted contribution to $F^{(1)}(z,t)$ as the second term in the first-pair brackets of (B.7) tends to decay exponentially with time. The integration over μ can be done if one notes the following straightforward integration

$$\int_0^c \frac{\mathrm{e}^{ax}}{b^{x/c}}\mathrm{d}x = \frac{c(\mathrm{e}^a - b^{1/c})}{\{ac - \ln(b)\}}. \tag{B.8}$$

Keeping only the most weighted term G_1 in (B.7) and use of (B.8) gives us

$$F^{(1)}(z,t) \approx \frac{2G_1 W_0 \lambda}{\beta}\cos^2\left(\frac{\lambda z}{2}\right)\mathrm{e}^{-S\,z} \times \left[\frac{\exp(W_0\lambda \mathrm{e}^{\beta t}/\beta) - \tan(\lambda z/2)}{W_0\lambda \mathrm{e}^{\beta t}/\beta - \ln[\tan(\lambda z/2)]}\right]. \tag{B.9}$$

References

Charney JG, Eliassen AA. 1964. On the growth of the hurricane depression. *J. Atmos. Sci.* **21**: 68–75.

Craig GC, Gray SL. 1996. CISK or WISHE as the mechanism for tropical cyclone intensification. *J. Atmos. Sci.* **53**: 3528–3540.

Emanuel KA. 1986. An air-sea interaction theory for tropical cyclone. Part I: Steady state maintenance. *J. Atmos. Sci.* **43**: 585–604.

Emanuel KA. 1989. The finite-amplitude nature of tropical cyclogenesis. *J. Atmos. Sci.* **46**: 3431–3456.

Eliassen AA. 1952. Slow thermally or frictionally controlled meridional circulation in a circular vortex. *Astrophys. Norv.* **5**: 19–60.

Gray WM. 1979. Hurricanes: Their formation, structure, and likely role in the tropical circulation. Pp 155–199 in *Meteorology over the Tropical Oceans*, Shaw DB (ed.) R. Meteorol. Soc: Reading, UK.

Hack JJ, Schubert WH. 1986. Nonlinear response of atmospheric vortices to heating by organized cumulus convection. *J. Atmos. Sci.* **43**: 1559–1573.

Heming JT. 2008. 'Tropical cyclone initialization in the Met Office global model: Is it still necessary and can it be improved?' In proceedings of 28th Conference on hurricanes and tropical meteorology, Orlando, Florida. Amer. Meteorol. Soc: Boston.

Heming JT, Radford AM. 1998. The performance of the UK Meteorological Office global model in predicting the tracks of Atlantic tropical cyclones in 1995. *Mon. Weather Rev.* **126**: 1323–1331.

Hendricks EA, Montgomery MT, Davis CA. 2004. The role of 'vortical' hot towers in the formation of tropical cyclone Diana (1984). *J. Atmos. Sci.* **61**: 1209–1232.

Holland G. 1997. The maximum potential intensity of tropical cyclones. *J. Atmos. Sci.* **54**: 2519–2541.

Kieu CQ, Zhang D-L. 2008. Genesis of tropical storm Eugene (2005) from merging vortices associated with the ITCZ breakdowns. Part I: Observational and modelling analyses. *J. Atmos. Sci.* **65**: 3419–3439.

Kurihara Y, Bender MA, Ross R. 1993. An initialization scheme of hurricane models by vortex specification. *Mon. Weather Rev.* **121**: 2030–2045.

Liu Y, Zhang D-L, Yau MK. 1997. A multiscale numerical study of hurricane Andrew (1992). Part I: Explicit simulation and verification. *Mon. Weather Rev.* **125**: 3073–3093.

Liu Y, Zhang D-L, Yau MK. 1999. A multiscale numerical study of hurricane Andrew (1992). Part II: Kinematics and inner-core structures. *Mon. Weather Rev.* **127**: 2597–2616.

McBride JL. 1981. Observational analysis of tropical cyclone formation. Part I: Basic description of data sets. *J. Atmos. Sci.* **38**: 1117–1131.

McBride JL, Zehr R. 1981. Observational analysis of tropical cyclone formation. Part II: Comparison of non-developing versus developing systems. *J. Atmos. Sci.* **38**: 1132–1151.

Montgomery MT, Nicholls ME, Cram TA, Saunders AB. 2006. A vortical hot tower route to tropical cyclogenesis. *J. Atmos. Sci.* **63**: 355–386.

Ooyama K. 1969. Numerical simulation of the life cycle of tropical cyclones. *J. Atmos. Sci.* **26**: 3–40.

Pandya RE, Durran DR. 1996. The influence of convectively generated thermal forcing on the mesoscale circulation around squall lines. *J. Atmos. Sci.* **53**: 2924–2951.

Pandya RE, Durran DR, Weisman ML. 2000. The influence of convective thermal forcing on the three-dimensional circulation around squall lines. *J. Atmos. Sci.* **57**: 29–45.

Polyanin AD, Zaitsev VF, Moussiaux A. 2001. *Handbook of First-Order Partial Differential Equations*. CRC Press.

Pu ZX, Braun SA. 2001. Evaluation of bogus vortex techniques with four-dimensional variational data assimilation. *Mon. Weather Rev.* **129**: 2023–2039.

Rodgers EB, Olson WS, Karyampudi VM, Pierce HF. 1998. Satellite-derived latent heating distribution and environmental influences in hurricane Opal (1995). *Mon. Weather Rev.* **126**: 1229–1247.

Rotunno R, Emanuel KA. 1987. An air–sea interaction theory for tropical cyclones. Part II: Evolutionary study using a nonhydrostatic axisymmetric numerical model. *J. Atmos. Sci.* **44**: 542–561.

Schubert WH, Hack JJ. 1982. Inertial stability and tropical cyclone development. *J. Atmos. Sci.* **39**: 1687–1697.

Shapiro LJ, Willoughby HE. 1982. The response of balanced hurricanes to local sources of heat and momentum. *J. Atmos. Sci.* **39**: 378–394.

Sundqvist H. 1970. Numerical simulation of the development of tropical cyclones with a ten-level model: I. *Tellus* **22**: 359–390.

Tao WK, Smith EA, Adler RF, Haddad ZS, Hou AY, Iguchi T, Kakar R, Krishnamurti TN, Kummerow CD, Lang S, Meneghini R, Nakamura K, Nakazawa T, Okamoto K, Olson WS, Satoh S, Shige S, Simpson J, Takayabu Y, Tripoli GJ, Yang S. 2006. Retrieval of latent heating from TRMM measurements. *Bull. Amer. Meteorol. Soc.* **87**: 1555–1572.

Wang D, Liang X, Zhao Y, Wang B. 2008. A comparison of two tropical cyclone bogussing schemes. *Weather Forecasting.* **23**: 194–204.

Wang Y. 1998. On the bogussing of tropical cyclones in numerical models: The influence of vertical structure. *Meteorol. Atmos. Phys.* **65**: 153–170.

Wang Y, Holland GJ. 1996. The beta drift of baroclinic vortices. Part I: Adiabatic vortices. *J. Atmos. Sci.* **53**: 411–427.

Willoughby HE. 1979. Forced secondary circulations in hurricanes. *J. Geophys. Res.* **84**: 3173–3183.

Willoughby HE. 1990a. Temporal changes of the primary circulation in tropical cyclones. *J. Atmos. Sci.* **47**: 242–264.

Willoughby HE. 1990b. Gradient balance in tropical cyclones. *J. Atmos. Sci.* **47**: 265–274.

Willoughby HE, Clos J, Shoreibah M. 1982. Concentric eye walls, secondary wind maxima, and the evolution of the hurricane vortex. *J. Atmos. Sci.* **39**: 395–411.

Xiao Q, Zou X, Wang B. 2000. Initialization and simulation of a landfalling hurricane using a variational bogus data assimilation scheme. *Mon. Weather Rev.* **128**: 2252–2269.

Yanai M. 1964. Formation of tropical cyclones. *Rev. Geophys.* **2**: 367–414.

Zhang D-L, Bao N. 1996. Oceanic cyclogenesis as induced by a mesoscale convective system moving offshore. Part II: Genesis and thermodynamic transformation. *Mon. Weather Rev.* **124**: 2206–2226.

DOI: 10.1002/qj

Zhang D-L, Kieu CQ. 2006. Potential vorticity diagnosis of a simulated hurricane. Part II: Quasi-balanced contributions to forced secondary circulations. *J. Atmos. Sci.* **63**: 2898–2914.
Zhang D-L, Liu Y, Yau MK. 1999. Surface winds at landfall of hurricane Andrew (1992) – A reply. *Mon. Weather Rev.* **127**: 1711–1721.
Zhang D-L, Liu Y, Yau MK. 2001. A multiscale numerical study of hurricane Andrew (1992). Part IV: Unbalanced flows. *Mon. Weather Rev.* **129**: 92–107.
Zhang D-L, Liu Y, Yau MK. 2002. A multiscale numerical study of hurricane Andrew (1992). Part V: Inner-core thermodynamics. *Mon. Weather Rev.* **130**: 2745–2763.
Zhu H, Smith RK, Ulrich W. 2001. A minimal three-dimensional tropical cyclone model. *J. Atmos. Sci.* **58**: 1924–1944.
Zhu T, Zhang D-L, Weng F. 2002. Impact of the Advanced Microwave Sounding Unit data on hurricane forecasts. *Mon. Weather Rev.* **130**: 2416–2432.

DOI: 10.1002/qj